PHYSICAL REVIEW B **76**, 245208 (2007)

# Raman scattering study of carrier-transport and phonon properties of 4*H*-SiC crystals with graded doping

S. Nakashima, T. Kitamura, T. Mitani,* and H. Okumura
*National Institute of Advanced Industrial Science and Technology, Power Electronics Research Center, 1-1-1 Umezono, Tsukuba, Ibaraki 305-8567, Japan*

M. Katsuno and N. Ohtani
*Advanced Technology Research Laboratories, Nippon Steel Corporation, 20-1 Shintomi, Futtsu, Chiba 293-8511, Japan*
(Received 12 June 2007; revised manuscript received 29 September 2007; published 21 December 2007)

Micro-Raman imaging measurements of *n*-type 4*H*-SiC crystals with graded donor concentration were carried out, and spatial distributions of the free carrier concentration, carrier mobility, and longitudinal optical (LO) phonon damping were obtained from a line shape analysis of the LO phonon-plasmon coupled (LOPC) mode. The damping of free carriers and optic phonons was determined as a function of free carrier density. We obtained an empirical relationship between carrier concentration and relative Raman shift of the LOPC mode, which is in close agreement with the relationship calculated for the damping-free coupled mode. It is found that the LO phonon damping deduced from the analysis increases linearly with carrier concentration. This LO mode behavior is mainly attributed to the interaction of the LO phonon and ionized impurities (free electrons).

DOI: 10.1103/PhysRevB.76.245208 PACS number(s): 78.30.−j, 73.61.Le, 73.50.Dn

## I. INTRODUCTION

In polar semiconductors, longitudinal optic phonon modes interact with the plasma oscillation of free carriers through their polarization fields and form LO phonon-plasmon coupled (LOPC) modes. By Raman scattering of this mode, phonon and electron properties of polar semiconductors, including III-V, II-VI, and IV-IV compounds, have been studied. The data on free carrier density and mobility have been extracted from a Raman line shape analysis of the LOPC modes using the classical dielectric function for the LO phonon-plasmon hybrid system.[1–8]

In III-V semiconductors such as GaAs, the damping of free carriers, $\gamma$, is usually small, and the frequency of the coupled modes varies sensitively with the plasma frequency $\omega_p$.[2] This behavior demonstrates that the coupled mode in GaAs has a strong plasmon character. In contrast, the carrier damping of wide-gap semiconductors such as SiC is large, and the plasmon is usually overdamped ($\omega_p \ll \gamma$). The frequency of the coupled modes in this system is close to the LO phonon frequency, and the LOPC mode in wide-gap semiconductors has a strong phonon character. Therefore, LO phonon damping should play an important role in the line shape analysis of the LOPC mode. However, in the earlier stages of Raman studies on the LOPC mode, only the damping of the TO phonon has been taken into account, and it has been treated as a frequency-dependent effective phonon damping in the analysis. Recently, an extended classical dielectric function that includes LO phonon damping along with TO phonon damping has been adopted for the LOPC mode analysis.[9–13] Nakashima and Harima showed that the incorporation of LO phonon damping into the dielectric function leads to a closer fit to the experimental Raman and infrared reflection spectra for 6*H*-SiC.[9] The analysis of LOPC modes using the extended dielectric function demonstrated that the LO phonon damping in 6*H*-SiC increases linearly with doping concentration of nitrogen or free carrier density.[10] The increase in damping of the LO phonon with increasing doping level was attributed to the Fröhlich-type interaction of the LO phonon with ionized impurities[14] and free electrons.

Previous studies of 6*H*-SiC crystals were insufficient to determine the carrier density and mobility with high accuracy since the frequency variation of the LOPC mode with free carrier density was extremely small. However, the electron mobility in 4*H*-SiC is higher than that in 6*H*-SiC; hence, the frequency variation of the LOPC mode with carrier concentration is large in 4*H*-SiC. This enables us to determine the variation in Raman parameters, such as the peak frequency, and LO phonon damping with higher accuracy.

When the plasma frequency is low and the coupled mode in the upper branch has a predominantly phonon character, the damping constants of the LO phonons and carriers contribute almost equally to the broadening of the LOPC mode, though $\gamma$ is related to the asymmetry of the LOPC mode. This situation is encountered in wide-gap semiconductors, such as SiC, GaN, and GaP, in which the carrier damping is relatively large. Hence, in the case of overdamped plasmon systems, it is necessary to choose the appropriate LO phonon damping to determine the electrical properties of wide-gap semiconductors accurately by the Raman spectroscopic technique. The importance of the LO phonon damping in the line shape fitting procedure has not yet been fully recognized. Furthermore, it is of great interest to study the electron-phonon interaction from the viewpoint of phonons. To date, phonon-electron interactions have only been treated from an electrical point of view through electrical measurements.

In the present work, we measured micro-Raman images of 4*H*-SiC crystals with graded donor concentrations. The carrier density, mobility, and LO phonon damping were determined from the LOPC analysis on the basis of the extended dielectric function. The LO phonon damping and carrier mobility were obtained as a function of carrier density. The mechanism for the LO phonon damping was discussed.

 ©2007 The American Physical Society

## II. THEORY OF RAMAN SCATTERING FROM THE LO PHONON-PLASMON COUPLED MODE

The Raman line shape of the LOPC modes has been studied theoretically and experimentally.[1–8] The line shape and frequency of the coupled modes have been calculated using dielectric analysis. The Raman scattering efficiency for the LOPC mode is given by[9]

$$W(\omega) = S[n(\omega)+1]A(\omega)\mathrm{Im}\left(\frac{-1}{\varepsilon_M(\omega)}\right), \tag{1}$$

where

$$A(\omega) = F_1(\omega) - \frac{\varepsilon_1(\omega)}{\varepsilon_2(\omega)}F_2(\omega), \tag{2}$$

$$\varepsilon_M(\omega) = \varepsilon_1(\omega) + i\varepsilon_2(\omega). \tag{3}$$

Most researchers have used a classical dielectric function, which is represented by the sum of the contributions from phonons and free carriers,

$$\varepsilon(\omega) = \varepsilon_\infty + \frac{(\varepsilon_0-\varepsilon_\infty)\omega_T^2}{\omega_T^2-\omega^2-i\Gamma_T\omega} - \frac{\varepsilon_\infty\omega_p^2}{\omega(\omega+i\gamma)}, \tag{4}$$

where $\omega_T$ is the frequency of TO phonons, and $\Gamma_T$ and $\gamma$ are damping constants of the TO phonons and carriers. The plasma frequency is related to the effective mass of carriers and carrier density by the following equation:

$$\omega_p^2 = \frac{4\pi n e^2}{\varepsilon_\infty m^*}. \tag{5}$$

In order to take into account the LO phonon damping adequately, we adopt the following dielectric function that incorporates the LO phonon damping,[9–13]

$$\frac{\varepsilon_M(\omega)}{\varepsilon_\infty} = \frac{\omega_L^2-\omega^2-i\Gamma_L\omega}{\omega_T^2-\omega^2-i\Gamma_T\omega} - \frac{\omega_p^2}{\omega(\omega+i\gamma)}, \tag{6}$$

where $\omega_L$ is the frequency of LO phonon. We shall hereafter refer to this function as the extended classical dielectric function (ECDF). This formula has been used for the analysis of Raman spectra[9,10] and infrared reflection spectra.[9,11–13] The real and imaginary parts of the above dielectric function are given by[9]

$$\varepsilon_1(\omega) = \varepsilon_\infty\left[\frac{(\omega_L^2-\omega^2)(\omega_T^2-\omega^2)+\omega^2\Gamma_T\Gamma_L}{(\omega_T^2-\omega^2)^2+(\omega\Gamma_T)^2} - \frac{\omega_p^2}{\omega^2+\gamma^2}\right]. \tag{7}$$

$$\varepsilon_2(\omega) = \varepsilon_\infty\left[\frac{\omega\Gamma_T(\omega_L^2-\omega^2)-\omega\Gamma_L(\omega_T^2-\omega^2)}{(\omega_T^2-\omega^2)^2+(\omega\Gamma_T)^2} + \frac{\omega_p^2\gamma}{\omega(\omega^2+\gamma^2)}\right]. \tag{8}$$

The exact forms of the functions $F_1$ and $F_2$ are as follows:

$$\begin{aligned} F_1(\omega) = {} & 1 + 2C\frac{\omega_T^2}{\omega_L^2-\omega_T^2}\frac{(\omega_L^2-\omega_T^2)(\omega_T^2-\omega^2)+\omega^2\Gamma_T(\Gamma_L-\Gamma_T)}{(\omega_T^2-\omega^2)+(\omega\Gamma_T)^2} \\ & - \frac{C^2\omega_T^4}{(\omega_L^2-\omega_T^2)^2} \\ & \times\left\{\left[\frac{(\omega_L^2-\omega_T^2)(\omega_T^2-\omega^2)+\omega^2\Gamma_T(\Gamma_L-\Gamma_T)}{(\omega_t^2-\omega^2)^2+(\omega\Gamma_T)^2}\right] \right. \\ & \times\left[1-\frac{\omega_p^2}{\omega^2+\gamma^2}\right] \\ & \left. - \frac{\omega\omega_p^2\gamma\Gamma_T(\omega_L^2-\omega_T^2)-\omega\omega_p^2\gamma(\Gamma_L-\Gamma_T)(\omega_T^2-\omega^2)}{\omega(\omega^2+\gamma^2)[(\omega_T^2-\omega^2)^2+(\omega\Gamma_T)^2]}\right\}, \end{aligned} \tag{9}$$

and

$$\begin{aligned} F_2(\omega) = {} & \mathrm{Im}(F) \\ = {} & 2C\frac{\omega_T^2}{\omega_L^2-\omega_T^2}\frac{\omega\Gamma_T(\omega_L^2-\omega_T^2)-\omega(\Gamma_L-\Gamma_T)(\omega_T^2-\omega^2)}{(\omega_T^2-\omega^2)^2+(\omega\Gamma_T)^2} \\ & + \frac{C^2\omega_T^4}{(\omega_L^2-\omega_T^2)^2} \\ & \times\left\{\frac{\omega_p^2\gamma(\omega_L^2-\omega_T^2)(\omega_T^2-\omega^2)+\omega^2\omega_p^2\gamma\Gamma_T(\Gamma_L-\Gamma_T)}{\omega(\omega^2+\gamma^2)[(\omega_T^2-\omega^2)^2+(\omega\Gamma_T)^2]} \right. \\ & + \left(1-\frac{\omega_p^2}{\omega^2+\gamma^2}\right) \\ & \left. \times\frac{\omega\Gamma_T(\omega_L^2-\omega_T^2)-\omega(\Gamma_L-\Gamma_T)(\omega_T^2-\omega^2)}{(\omega_T^2-\omega^2)^2+(\omega\Gamma_T)^2}\right\}, \end{aligned} \tag{10}$$

where $C$ is the Faust-Henry coefficient.[15] When we set $\Gamma_L = \Gamma_T$, Eqs. (9) and (10) are reduced to the conventional expression derived from the classical dielectric function [Eq. (4)].

We have fitted Eqs. (1), (7), and (8) to observed LOPC mode profiles using $\omega_p$, $\gamma$, and $\Gamma_L$ as adjustable parameters. We need the other material parameters, viz., $\omega_L$, $\omega_T$, $\varepsilon_\infty$, $C$, and $m^*$, in addition to $\omega_p$, $\gamma$, $\Gamma_L$, and $\Gamma_T$. The values of $\omega_T$, $\varepsilon_\infty$, and $C$ are taken from Ref. 8. The carrier mobility is expressed as a function of carrier damping via

$$\mu = \frac{e}{m^*\gamma}. \tag{11}$$

For the electronic term in Eq. (4), a dielectric function based on the hydrodynamical model has been employed as an extension of the Drude theory by several researchers.[16–18] After expanding this function in $q/\omega$ we get a Drude form with wave-vector-dependent plasma frequency $\omega^2(q)=\omega_p^2[1+\langle v^2\rangle(q/\omega)^2]$, where $\langle v^2\rangle$ is the mean square of the carrier velocity. The Lindhard-Mermin dielectric function,[19] which was successfully used for heavily doped semiconductors, was also applied to a Raman analysis by several authors.[20–23] The small-$q$ and high-$\omega$ limit of the Lindhard Mermin susceptibility again leads to the Drude form with a $q$-dependent plasma frequency,[23]

$$\chi_e^{(\mathrm{LM})} \approx -\frac{\varepsilon_\infty}{4\pi}\frac{\omega_p^2[1+\langle v^2\rangle(q/\omega)^2]}{\omega(\omega+i\gamma)}. \quad (12)$$

The Drude function with a wave-vector-dependent term may yield a carrier-density difference of several tens of percent compared to the case without this term. Since in the SiC specimens used in this work, the free carrier concentration is not high and the system is not degenerated, the contribution of the dispersion effect might be small.

Another dielectric function obtained by extending the generalized Lyddane-Sachs-Teller (LST) relation to the plasmon-phonon coupled system[24–27] is given by the following equation:

$$\varepsilon_k(\omega) = \frac{\varepsilon_\infty(\omega^2-\omega_1^2+i\gamma_1\omega)(\omega^2-\omega_2^2+i\gamma_2\omega)}{\omega(\omega+i\gamma_p)(\omega^2-\omega_T^2+i\Gamma_T\omega)}, \quad (13)$$

where $\omega_1$ and $\omega_2$ are the frequencies of the upper and lower branches of the LOPC mode, respectively, and $\gamma_1$ and $\gamma_2$ are the damping constants of these modes. Equation (13) assumes that the coupled mode decays directly through the lower and upper modes themselves. In contrast, Eqs. (4) and (6) are based on the model that the LOPC mode is formed from the coupling of the decaying LO phonon system and damping plasmon system and that the relaxation of the coupled mode occurs through each channel of the phonon and electron systems. It has been reported that spectral analysis using Eq. (13) gave a good agreement with experimental reflection spectra.[24,27] However, since there was no theoretical work relating the damping constants $\gamma_1$ and $\gamma_2$ to measurable physical quantities, this equation has not been widely used.

The equivalence of Eqs. (4) and (13) has been discussed by Sievers and Page[28] and Berreman and Unterwald,[29] who argued that the dielectric function with the factorized form can be modified to a classical oscillator model under some restrictions by use of the LST relation.

When $\omega_p \ll \omega_L$ or $\omega_p \gg \omega_L$ using the relation $\omega_1^2+\omega_2^2=\omega_p^2+\omega_L^2$ for a small damping case, Eq. (13) can be rewritten as

$$\varepsilon_M(\omega) \approx \frac{\varepsilon_\infty(\omega_L^2-\omega^2-i\gamma_1\omega)(\omega_p^2-\omega^2-i\gamma_2\omega)}{\omega(\omega+i\gamma_p)(\omega^2-\omega_T^2+i\Gamma_T\omega)}. \quad (14)$$

Expanding the numerator and denominator of this equation in terms of powers of $\omega^2$ for larger $\omega$ and neglecting terms of order $\omega^{-4}$, we obtain

$$\varepsilon_M(\omega) \approx \varepsilon_\infty + \frac{\varepsilon_\infty(\omega_L^2-\omega_T^2)}{\omega_T^2-\omega^2-i\Gamma_T\omega} - \frac{\varepsilon_\infty\omega_p^2}{\omega(\omega+i\gamma)} + iO(\omega^{-1}). \quad (15)$$

The approximate coincidence of the two dielectric functions would validate the use of the dielectric function with additive form for the LOPC mode analysis.

## III. EXPERIMENT

### A. Sample preparation

4*H*-SiC crystals were grown by the modified-Lely method. The growth direction was ⟨1-100⟩. Graded doping of

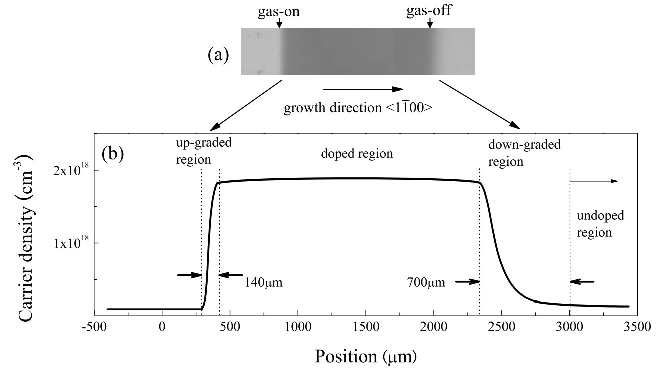


FIG. 1. (a) Micrograph of graded doping sample. (b) Distribution of free carrier density in the sample.

nitrogen was achieved by repeatedly switching the $N_2$ gas supply on and off.[30] The growth rate of the crystal was approximately 1 mm/h. A sample with the (0001) surface was cut out from an ingot and polished optically flat.

Figure 1(a) shows an optical micrograph of the (0001) cross section, which reveals an inhomogeneous distribution of the N dopant. The dark region is doped with N donors. Figure 1(b) shows the distribution of free carrier densities determined from the Raman analysis of the image measurements of the LOPC mode, as will be described later on. The free carrier concentration, i.e., donor concentration, varies in space after opening and closing the gas supply. The graded doping regions obtained upon switching the $N_2$ gas supply on and off will be called "upgraded region" and "downgraded region," respectively. The thicknesses of the up- and downgraded regions are about 140 and 700 $\mu$m, respectively. A gradual decrease of the nitrogen gas concentration in the furnace after shutting the doping gas causes the downgraded region to thicken compared with the upgraded region. The carrier concentration $n$ was $(3-4)\times 10^{18}$ cm$^{-3}$ in the doped region and $(2-3)\times 10^{17}$ cm$^{-3}$ in the undoped region.

### B. Raman microprobe measurements

Micro-Raman images of the $A_1$-LOPC mode were obtained at room temperature using a Raman microprobe. A laser beam with $\lambda=457.9$ nm was expanded linearly with a cylindrical lens placed in front of the microscope and hit the (0001) surfaces.

The linearly expanded laser beam was focused to $1\times 500$ $\mu$m$^2$ on the sample surface through an objective lens with a numerical aperture of 0.3. The scattered light was dispersed by a double monochromator ($f=1.0$ m), and the Raman image was detected by a cooled charge coupled device detector with $400\times 1340$ pixels. The spatial resolution limited by the finite pixel size ($20\times 20$ $\mu$m$^2$) was 2 $\mu$m (in the $y$ direction), and the spectral resolution (in the $x$ direction) was 0.2 cm$^{-1}$.

## IV. RESULTS AND DISCUSSION

### A. Raman peak shift of the LO phonon-plasmon coupled mode with carrier density

A one-dimensional Raman image of the $A_1$-LOPC modes along the growth direction ⟨1-100⟩ is obtained for an up-

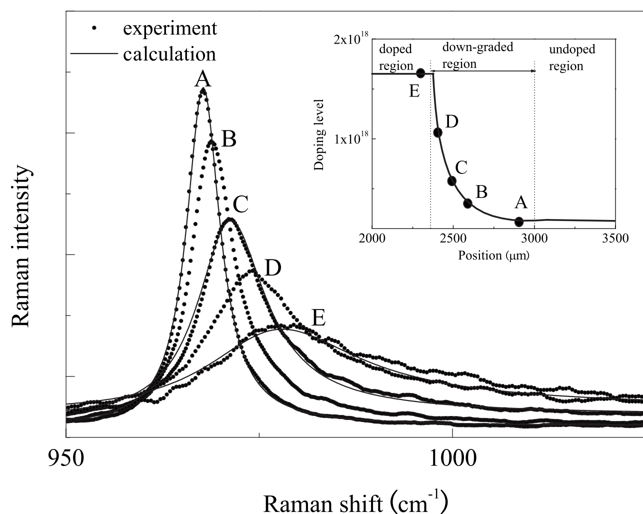


FIG. 2. Raman spectra of the LOPC mode at typical positions in the graded doping region of 4$H$-SiC. The solid lines show fitted curves calculated using Eqs. (1), (7), and (8).

graded region. The LOPC mode spectra showed a monotonic variation of the peak frequency in the up- and downgraded doping regions, while no appreciable frequency change was observed for the TO ($E_2$) mode at 776 $\mathrm{cm}^{-1}$. In Fig. 2, we show the Raman line shape of the LOPC mode for typical positions in the downgraded region, as shown in the inset.

The fit to the observed line shape of the LOPC mode was made by a nonlinear least squares fit program using the ECDF of Eq. (6). The parameters assumed known were $m_{\parallel}^{*}$, $\varepsilon_0$, $\varepsilon_\infty$, $\omega_T$, $\omega_L$, and $\Gamma_T$. The program varied three parameters: $\omega_p$, $\gamma$, and $\Gamma_L$. We set $\omega_T=783$ $\mathrm{cm}^{-1}$ and $\Gamma_T=2.1$ $\mathrm{cm}^{-1}$ for the $A_1$(TO) mode, and $\omega_L=964.1$ $\mathrm{cm}^{-1}$ for the $A_1$(LO) mode. The effective mass relevant to the present experiment is the mass parallel to the $c$ axis. This longitudinal effective mass is taken as $m_{\parallel}^{*}=0.29m_0$,[31] where $m_0$ is the free electron mass. The carrier density $n$ and mobility $\mu$ were obtained from the best-fit parameters $\omega_p$ and $\gamma$ using Eqs. (5) and (11).

The local carrier concentration in the graded region and the peak frequency of the LOPC mode were determined as a function of position from the analysis of the Raman image for the LOPC mode. In the sequential fitting for series of the data in the graded region, special care was needed. The LO phonon damping $\Gamma_L$ and carrier damping $\gamma$ contribute equivalently to the broadening of the LOPC mode, and the two parameters play similar roles in the line shape fitting, although $\gamma$ is related to the asymmetry of the LOPC mode. However, the two damping constants give reverse effects on the peak frequency of this band: The increase of $\gamma$ provides a downshift of the band, while the increase of $\Gamma_L$ provides an upshift of the LOPC band in low carrier-density regime. This situation is favorable for reducing the uncertainty in determination of $\gamma$ and $\Gamma_L$ by fitting. In the fitting procedure, we have determined $\gamma$'s and $\Gamma_L$'s so that (i) $\Gamma_L$ increases with increasing carrier density $n$, (ii) the intercept of $\Gamma_L$ (at $n=0$) is close to the intrinsic Raman width, and (iii) the fitted mobilities take physically meaning $n$ dependence. We have chosen the best-fit parameters of $\gamma$ and $\Gamma_L$ determined under the above constraints.

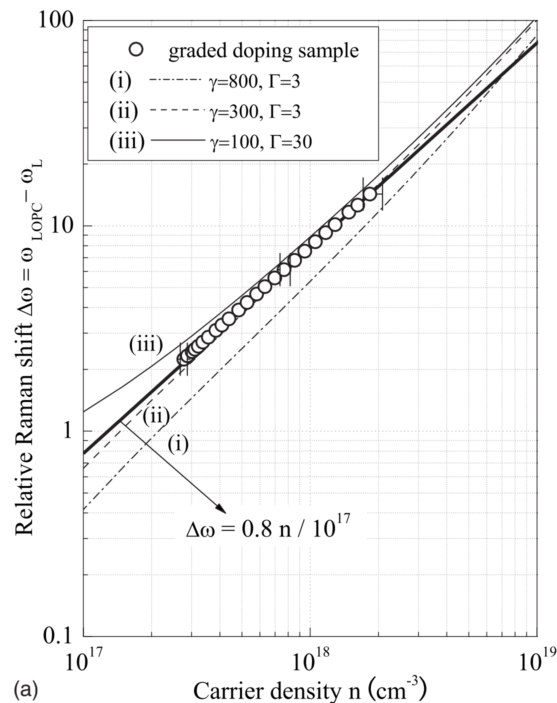


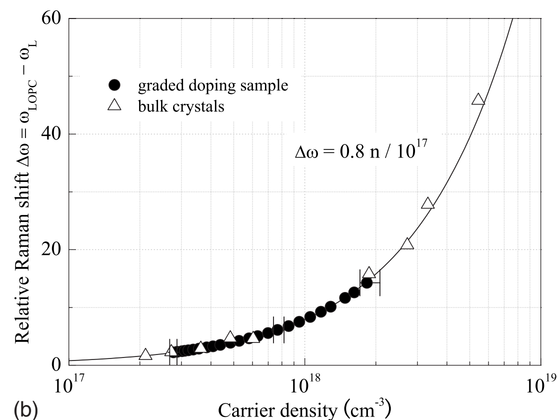


FIG. 3. (a) The relative Raman shift $\Delta\omega$ as a function of the free carrier density $n$. The $\Delta\omega$-$n$ relation calculated for (i) $\gamma=800$ and $\Gamma_L=3$, (ii) $\gamma=300$ and $\Gamma_L=3$, and (iii) $\gamma=100$ and $\Gamma_L=30$ are shown for comparison. (b) The relation between $\Delta\omega$ $(=\omega_{\mathrm{LOPC}}-\omega_L)$ and $n$ for graded doping specimens and various bulk crystals. The solid line is a curve given by Eq. (16).

In Fig. 3(a), we plot the peak frequency of the LOPC mode as a function of the carrier concentration on a logarithmic scale. This figure demonstrates that there is a very simple relationship between the carrier concentration and the LOPC mode frequency relative to the bare LO phonon frequency in pure 4$H$-SiC in units of $\mathrm{cm}^{-1}$,

$$n = 1.25 \times 10^{17}(\mathrm{cm}^{-3})(\omega_{\mathrm{LOPC}} - \omega_L)^{1.0} = 1.25 \times 10^{17}(\Delta\omega)^{1.0}. \quad (16)$$

An empirical relation similar to the above relation has been obtained for GaN, for which the exponent of $\Delta\omega$ was found to be 0.764.[32] That the exponent for GaN is smaller reflects

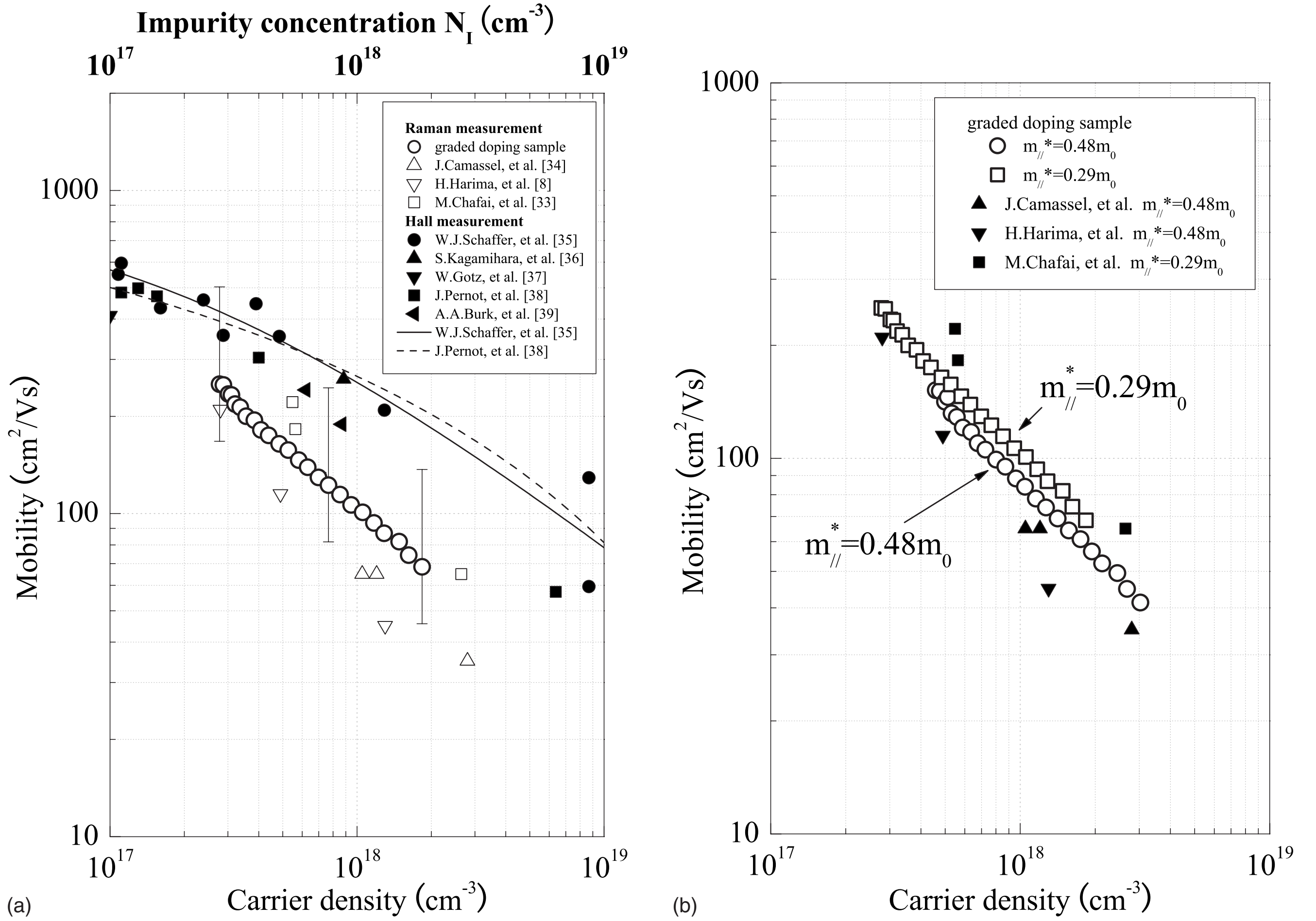


FIG. 4. (a) The carrier mobility determined from the line shape analysis of the LOPC mode in graded-doped 4$H$-SiC is plotted as a function of $n$. The effective mass is taken as $m^*=0.29m_0$ for this Raman analysis. The Hall mobilities as measured by various authors are shown for comparison. The Hall mobility is plotted against impurity concentration. The empirical $\mu$-$n$ relations (solid and broken lines) are obtained from Refs. 35 and 36, respectively. The error bars for mobility data account for the uncertainty in the determination of $\gamma$ by the line shape fitting. (b) The $\mu$-$n$ relation calculated by means of the LOPC analysis for $m^*=0.29m_0$ is compared with that of $m^*=0.48m_0$ for graded-doped 4$H$-SiC. Raman data obtained for several bulk samples are also shown for comparison.

the fact that the plasma frequency $\omega_p$ in GaN, studied by Wetzel *et al.*,[32] is comparable to the LO phonon frequency and that the peak frequency of the LOPC mode in GaN is more sensitive to the change in carrier density.

The relationship between the carrier concentration and the relative Raman frequency $\Delta\omega$ can be easily derived for small damping of the phonon and carriers. For coupled modes with a negligibly small damping of carriers and phonons, the frequency of the upper mode $\omega_+$ is given as a solution of $\varepsilon(\omega)=0$ in Eq. (4),

$$\frac{\omega_+^2-\omega_L^2}{\omega_+^2-\omega_T^2}=\frac{\omega_p^2}{\omega_+^2}. \tag{17}$$

For the phononlike coupled mode with a moderate carrier concentration, we may substitute

$$\omega_+^2-\omega_L^2=(\omega_++\omega_L)(\omega_+-\omega_L)\approx 2\Delta\omega\omega_L. \tag{18}$$

Since $\omega_p^2$, $(\Delta\omega)^2 \ll \omega_L^2$, $\omega_T^2$, $(\omega_L^2-\omega_T^2)$ for lightly doped SiC, we obtain the approximation $\omega_p^2\approx 2\omega_L(1-\varepsilon_\infty/\varepsilon_0)^{-1}\Delta\omega$, which leads to

$$n\approx\frac{\varepsilon_\infty m^*}{4\pi e^2}\frac{2\omega_L}{(1-\varepsilon_\infty/\varepsilon_0)}\Delta\omega. \tag{19}$$

Taking numerical values of the parameters and $m^*=0.29m_0$ in 4$H$-SiC, the above equation gives $n=1.23\times 10^{17}$ $\Delta\omega$ which quite agrees with the empirical relation [Eq. (16)]. In Fig. 3(a), we also plot $\Delta\omega$-$n$ curves calculated for given damping constants for carriers and LO phonons. As shown in this figure, the larger the damping of free carriers, the lower the relative Raman shift $\Delta\omega$ at a given $n$, while larger damping of the LO phonon results in larger $\Delta\omega$ values. The experimentally observed linear relationship between $\Delta\omega$ and $n$ in Fig. 3(a) is presumably due to the reverse effects of the damping of the LO phonon and carrier on $\Delta\omega$. The $\Delta\omega$ vs $n$ curve given by Eq. (19) lies between the two curves for (ii) $\gamma=300$ cm$^{-1}$, $\Gamma_L=3$ cm$^{-1}$ and (iii) $\gamma=100$ cm$^{-1}$, $\Gamma_L=30$ cm$^{-1}$. This implies that determining the carrier density from the LOPC analysis requires taking into account the damping of carriers and LO phonons. A change of free carrier concentration by $1\times 10^{17}$ cm$^{-3}$ corresponds to a fre-

quency variation of $\Delta\omega=0.8\ \mathrm{cm}^{-1}$ in the concentration range from $1\times10^{17}$ to $4\times10^{18}\ \mathrm{cm}^{-3}$. Thus, precise measurement of the peak frequency of the LOPC mode is needed to determine the carrier concentration at low carrier concentrations between $10^{17}$ and $10^{18}\ \mathrm{cm}^{-3}$. The empirical relationship for carrier density and relative Raman shift holds not only for graded doping SiC, but also for various bulk materials. We have also measured the Raman spectra of the LOPC mode in 4*H*-SiC bulk crystals grown in various institutes and have determined the carrier density. Figure 3(b) compares the results with the data obtained for the graded doping specimens. One can see that the empirical relation Eq. (16) still holds in the carrier-density range of $10^{17}-10^{19}\ \mathrm{cm}^{-3}$. The relationship between $n$ and the LOPC mode frequency was shown graphically by Harima *et al.*[8] and Chafai *et al.*,[33] though their functional forms were not given.

### B. Carrier-density dependence of mobility

The carrier mobility deduced from the best-fit value of the carrier damping using Eq. (11) is plotted as a function of carrier density in Fig. 4(a). The carrier-density dependence of the mobility shows almost the same trend as that in previous results obtained by Raman analysis on 4*H*-SiC bulk crystals.[8,33,34] The Hall mobility of 4*H*-SiC has been measured for epitaxial films by many researchers. In Fig. 4(a), the mobilities derived from d.c. measurements[35–39] are shown for various impurity concentrations. Kagamihara *et al.*[36] and Pernot *et al.*[38] obtained the relationship between the mobility and impurity concentration $N_I$ on the basis of results of electrical measurements, which are also shown in Fig. 4(a). The dc mobility values ($\mu_{\mathrm{dc}}$) derived from their empirical relations seem to be somewhat large as compared with the ones deduced from Raman analysis even when we plot $\mu_{\mathrm{dc}}$ against $n$ instead of the dopant concentration $N_I$ assuming that $n$ is smaller than $N_I$.

Several reasons can account for this discrepancy.

(i) The question may arise as to whether the carrier mobility depends on the effective mass value employed. We have used the optical effective mass of $m^*=0.29m_0$ for 4*H*-SiC, which has more recently been obtained from optical detection of cyclotron resonance measurements.[31] Meanwhile, the value of $m^*=0.48m_0$ was used in our previous Raman study.[8] Using this value, we calculated the $\mu$-$n$ relation, the result of which is compared with the relation for $m^*=0.29m_0$ in Fig. 4(b). We can see that there is no appreciable difference in the $\mu$-$n$ curve for $m^*=0.29m_0$ and $m^*=0.48m_0$, though at a given $\omega_p$, the mobility and carrier concentration differ for these effective masses because $\omega_p^2$ is proportional to $n/m^*$. This suggests that the choice of the effective mass is not responsible for the difference observed in the $\mu$-$n$ relationship between Hall and optical measurements.

(ii) It should be noted that the Hall mobility in Fig. 4(a) was obtained for epitaxial films, while the optical mobility was obtained for bulk crystals. There is a common opinion that the mobility in bulk SiC crystals is lower than in epitaxial films grown by the chemical vapor deposition method because the defect density may, in general, be higher for bulk

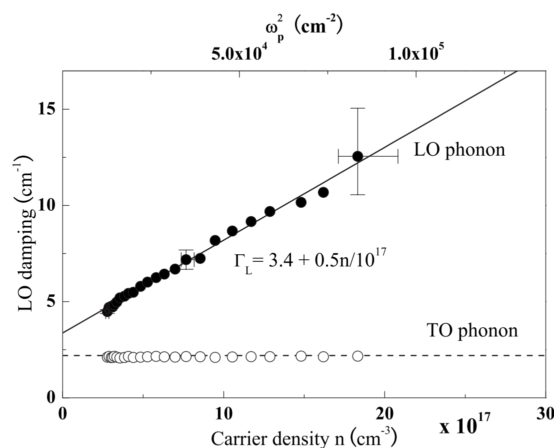


FIG. 5. The damping of the $A_1$(LO) phonon and $E_2$(TO) phonon is plotted as a function of the free carrier concentration for graded-doped 4*H*-SiC. The electron effective mass is taken as $m^*=0.29m_0$ in the Raman analysis.

samples. However, a quantitative comparison of the mobilities obtained from the two methods has not been reported.

(iii) For wide-gap semiconductors, including SiC,[8,34] GaN,[40–42] and ZnO,[43] the optical mobilities estimated from Raman scattering and infrared reflection measurements have been compared with that obtained from dc electrical measurements, though systematic studies have not yet been made. Most papers have reported that the optically determined carrier mobility is comparable to that determined from dc electrical measurements. However, recent experiments on GaN showed that IR and Raman mobilities are smaller than the Hall mobility.[40,41] Relaxation of phononlike LOPC modes has recently been investigated in GaAs by Vallée *et al.*,[44] whose theoretical model indicates that the relaxation time of carriers in the high frequency regime $\langle\tau\rangle_\infty$ is smaller than those deduced from Hall mobility measurements. On the basis of the above, the lowering of the optical mobility observed in wide-gap semiconductors may be partly due to the $\omega$ dependence of carrier relaxation time.

### C. LO phonon damping vs carrier density

Figure 5 plots the LO phonon damping $\Gamma_L$ derived from the line shape analysis of the LOPC mode as a function of carrier density. In this case, we take $m^*=0.29m_0$. As can be seen in this figure, $\Gamma_L$ varies linearly with carrier concentration, which is expressed in units of $\mathrm{cm}^{-1}$ as

$$\Gamma_L=\Gamma_0+an=3.4+0.5n/10^{17}\ \mathrm{cm}^{-3}. \tag{20}$$

The first term ($\Gamma_0$) corresponds to the intrinsic damping arising from phonon-phonon interaction (anharmonic potential). The bandwidth of the $A_1$-LO mode measured for pure 4*H*-SiC ($n=5\times10^{14}\ \mathrm{cm}^{-3}$) was $3.4\ \mathrm{cm}^{-1}$. The TO ($E_2$) band at $776\ \mathrm{cm}^{-1}$ was also measured in the graded doping region. As shown in Fig. 5, the width of the TO bands was independent of the carrier density and almost constant at $2.1\ \mathrm{cm}^{-1}$ in the concentration range measured in this work (from $3\times10^{17}$ to $2\times10^{18}\ \mathrm{cm}^{-3}$). This demonstrates that the linear

dependence of LO phonon damping on carrier density may be interpreted in terms of the Fröhlich-type interaction of LO phonons with ionized impurities and/or free electrons. It is of interest to compare the LO phonon damping $\Gamma_L$ for 4*H*-SiC with the result for 6*H*-SiC,[10] where $\Gamma_L$ is given by $\Gamma_L=\Gamma_0+0.32n/10^{17}\ \mathrm{cm}^{-3}$, for which the coefficient $a$ is slightly lower than that of 4*H*-SiC.

Ridley and Gupta[14] pointed out that ionized impurity scattering is important for the momentum relaxation of LO phonons in heavily doped semiconductors and that the damping of the LO phonon by this scattering mechanism is proportional to the ionized impurity concentration $N_I$. When the compensation ratio is small, the free carrier concentration is comparable to the concentration of donor impurity. Thus, the damping arising from LO phonon-electron scattering is expected to be proportional to $n$ and related to the Fröhlich coupling constant, $\alpha=[(2\pi e^2\hbar\omega_L)(1/\varepsilon_\infty-1/\varepsilon_0)]^{1/2}$. As mentioned before, the experimentally determined LO phonon damping is proportional to the carrier density for 4*H*- and 6*H*-SiC. When we assume that ionized impurity scattering is the dominant relaxation process, the coefficient $a$ should be the same for 4*H*- and 6*H*-SiC because the Fröhlich coupling constant is almost the same for both polytypes, and the damping constant does not depend on the effective mass of the free carriers. In contrast, when free carrier scattering governs the LO phonon relaxation, $a$ should depend on the effective mass value, which is different for 4*H*- and 6*H*-SiC. The behavior of LO phonon damping for 4*H*- and 6*H*-SiC may indicate that scattering by ionized impurities and free carriers contributes to the relaxation of the LO phonons in lightly doped SiC. However, it remains unclear which of the two mechanisms is predominant. More detailed theoretical work on the interaction of LO phonons with charged particles needs to be done before the predominant relaxation mechanism can be identified.

## V. SUMMARY

Micro-Raman measurements were carried out on 4*H*-SiC with graded carrier concentration. From the line shape analysis of the LOPC mode using the extended dielectric function, which includes LO phonon damping, the distribution of free carrier density, carrier mobility along the $c$ axis, and LO phonon damping were determined. This yielded the carrier mobility and LO phonon damping as a function of carrier density. The LO phonon damping was found to increase linearly with carrier concentration. This finding indicates that LO phonon decay occurs by ionized impurity scattering and free electron scattering. We found a simple relationship between the carrier concentration and relative Raman shift of the LOPC mode that will provide an easy way to determine the free carrier density in 4*H*-SiC.

## ACKNOWLEDGMENTS

The authors would like to thank T. Yamamoto for the technical assistance he offered in the early stages of this work. They are also indebted to H. Harima for providing them with the software for the LOPC analysis.

---

*Present address: Toray Research Center, Sonoyama, Otsu, Shiga, Japan.


[1] D. T. Hon and W. L. Faust, Appl. Phys. **1**, 241 (1973).
[2] M. V. Klein, in *Light Scattering in Solids*, edited by M. Cardona (Splinger, Berlim, 1975), Vol. 1.
[3] G. Irmer, V. V. Toporov, B. H. Bairamov, and J. Monecke, Phys. Status Solidi B **119**, 595 (1983).
[4] H. Yugami, S. Nakashima, and A. Mitsuishi, J. Appl. Phys. **61**, 354 (1987).
[5] P. J. Colwell and M. V. Klein, Phys. Rev. B **6**, 498 (1972).
[6] M. V. Klein, B. N. Ganguly, and P. J. Colwell, Phys. Rev. B **6**, 2380 (1972).
[7] R. Fukasawa and S. Perkowitz, Phys. Rev. B **50**, 14119 (1994).
[8] H. Harima, S. Nakashima, and T. Uemura, J. Appl. Phys. **78**, 1996 (1995).
[9] S. Nakashima and H. Harima, J. Appl. Phys. **95**, 3541 (2004).
[10] S. Nakashima, H. Harima, N. Ohtani, and M. Katsuno, J. Appl. Phys. **95**, 3547 (2004).
[11] J.-F. Baumard and F. Gervais, Phys. Rev. B **15**, 2316 (1977).
[12] F. Gervais, Phys. Rev. B **23**, 6580 (1981).
[13] E. Neyret, G. Ferro, S. Juillaguet, J. M. Bluet, C. Jaussaud, and J. Camassel, Mater. Sci. Eng., B **B61-62**, 253 (1999).
[14] B. K. Ridley and R. Gupta, Phys. Rev. B **43**, 4939 (1991).
[15] W. L. Faust and C. H. Henry, Phys. Rev. Lett. **17**, 1265 (1966).
[16] U. Nowak, W. Richter, and G. Sachs, Phys. Status Solidi B **108**, 131 (1981).
[17] T. Nakamura and T. Katoda, J. Appl. Phys. **55**, 3064 (1984).
[18] J. Ibáñez, R. Cuscó, and L. Atrús, Phys. Status Solidi B **223**, 715 (2001).
[19] N. D. Mermin, Phys. Rev. B **1**, 2362 (1970).
[20] G. Abstreiter, R. Trommer, M. Cardona, and A. Pinczuk, Solid State Commun. **30**, 703 (1979).
[21] K. Wan and J. F. Young, Phys. Rev. B **41**, 10772 (1990).
[22] R. Cuscó, J. Ibáñez, and L. Artús, Phys. Rev. B **57**, 12197 (1998).
[23] L. Artús, R. Cuscó, J. Ibáñez, N. Blanco, and G. González-Díaz, Phys. Rev. B **60**, 5456 (1999).
[24] A. A. Kukharskii, Sov. Phys. Solid State **14**, 1501 (1972).
[25] A. A. Kukharskii, Solid State Commun. **13**, 1761 (1973).
[26] S. Perkowitz and R. H. Thorland, Solid State Commun. **16**, 1093 (1975).
[27] S. Perkowitz, Phys. Rev. B **12**, 3210 (1975).
[28] A. J. Sievers and J. B. Page, Phys. Rev. B **41**, 3455 (1990).
[29] D. W. Berreman and F. C. Unterwald, Phys. Rev. **174**, 791 (1968).
[30] M. Katsuno, N. Ohtani, J. Takahashi, H. Yashiro, and M. Kanaya, Jpn. J. Appl. Phys., Part 1 **38**, 4661 (1999).
[31] N. T. Son, W. N. Chen, O. Kordina, A. O. Konstantinov, B. Monemar, E. Janzén, D. M. Hofman, D. Volm, M. Drechsler, and B. K. Meyer, Appl. Phys. Lett. **66**, 1074 (1995).
[32] C. Wetzel, W. Walukiewicz, E. E. Haller, J. Ager III, I. Grzegory,

S. Porowski, and T. Suski, Phys. Rev. B **53**, 1322 (1996).
[33] M. Chafai, A. Jaouhari, A. Torres, R. Antón, E. Martín, J. Jiménez, and W. C. Mitchel, J. Appl. Phys. **90**, 5211 (2001).
[34] J. Camassel, S. Juillaguet, N. Planes, A. Raymond, P. Grosse, G. Basset, C. Faure, M. Couchaud, J. M. Bluet, K. Chourou, M. Anikin, and R. Madar, Mater. Sci. Eng., B **B61-62**, 258 (1999).
[35] W. J. Schaffer, G. H. Negley, K. G. Irvine, and J. W. Palmour, Mater. Res. Soc. Symp. Proc. **339**, 595 (1994).
[36] S. Kagamihara, H. Matsuura, T. Hatakeyama, T. Watanabe, M. Kushibe, T. Shinohe, and K. Arai, J. Appl. Phys. **96**, 5601 (2004).
[37] W. Götz, A. Schöner, G. Pensl, W. Suttrop, W. J. Choyke, R. Stein, and S. Leibenzeder, J. Appl. Phys. **73**, 3332 (1993).
[38] J. Pernot, S. Contreras, J. Camassel, J. L. Robert, W. Zawadzki, E. Neyret, and L. Di Cioccio, Appl. Phys. Lett. **77**, 4359 (2000).
[39] A. A. Burk, Jr., M. J. O'Loughlin, R. R. Siergiej, A. K. Agarwal, S. Sriram, R. C. Clarke, M. F. MacMillan, V. Balakrishna, and C. D. Brandt, Solid-State Electron. **43**, 1459 (1999).
[40] T. Kozawa, T. Kachi, H. Kano, Y. Taga, M. Hashimoto, N. Koide, and K. Manabe, J. Appl. Phys. **75**, 1098 (1994).
[41] Z.-F. Li, W. Lu, H.-J. Ye, Z.-H. Chen, X.-Z. Yuan, H.-F. Dou, S.-C. Shen, G. Li, and S. J. Chua, J. Appl. Phys. **86**, 2691 (1999).
[42] G. Bentoumi, A. Deneuville, E. Bustarret, B. Daudin, G. Feuillet, E. Martinez, P. Aboughe-Nze, and Y. Monteil, Thin Solid Films **364**, 107 (2000).
[43] S. Brehme, F. Fenske, W. Fuhs, E. Nebauer, M. Poschenrieder, B. Selle, and I. Sieber, Thin Solid Films **342**, 167 (1999).
[44] F. Vallée, F. Ganikhanov, and F. Bogani, Phys. Rev. B **56**, 13141 (1997).